Design comparison and magnetic control of negative permeability metamaterials

JIUN-YEU CHEN, JIA-YI YEH[a], LIEN-WEN CHEN[b,*]
Center for General Education, Hsing Kuo University of Management, Tainan 709, Taiwan
[a]Department of Management Information Science, Chung Hwa University of Medical Technology, Tainan 717, Taiwan
[b]Department of Mechanical Engineering, National Cheng Kung University, Tainan 701, Taiwan

Four types of split ring resonators (SRRs), the so-called single-slit SRRs, two-slit SRRs (TSRRs), double-ring SRRs, and modified SRRs, have been considered and numerically investigated for the comparative analysis in connection with their suitability to the design of tunable metamaterials. It is found that the TSSR configuration on the gigahertz resonance reveals a larger variation in the magnetic resonance frequency through the influences of the SRR size scaling, the slit width and the substrate permittivity. Based on the TSRR structure infiltrated with liquid crystals (LCs) in the sandwich substrate, a tunable magnetic metamaterial was proposed in this study. The main relevant contribution of this paper is to provide a tuning procedure via controlling the director orientation of anisotropic LCs and to show that the TSRR structure can be designed to exhibit negative permeability over a broad frequency interval. The magnetic resonance frequencies could be adjusted in the microwave range of about 7.82 to 8.92 GHz.

(Received December 2, 2009; accepted March 16, 2011)

Keywords: Single negative media, Negative magnetic permeability, Liquid crystals, Tunable split-ring resonators (SRRs)

1. Introduction

A metamaterial is an artificially composite structure with effective electromagnetic properties which can be tailored by geometrical textures. An array of split ring resonators (SRRs), which exhibits negative permeability near its resonance frequency, has been successfully applied to the fabrication of left-handed metamaterials (LHMs). It has been verified that an array of wires and SRRs possesses all the non-intuitive features, including negative refraction, evanescent wave enhancement, and negative group velocity [1]. In the various designs of the rings, the main consideration of the resonant structures is that the wavelength must be much larger than the size of the scattering elements. This quasi-static resonance is different from the Bragg resonance which results from the periodic structure with a spatial scale on the order of the wavelength for the propagating radiation at resonance [2].

The properties of LHMs defined by composites are not determined by the essential physical properties of their constituents but by the shape and distribution of the resonant structures. One of the advantages for such artificial materials is the possibility of varying the entire properties by simply changing the SRR geometries of the unit cell [3-9]. In most of these cases, the resulting electromagnetic properties tend to be fixed after fabrication. However, as the left-handed passband frequency is essentially determined by the magnetic resonance frequency of the periodic ring structures, all the metamaterial-based devices, such as filters, amplifiers, antennas, sub-diffraction-limited hyperlenses, and cloaks [10-13], are limited to a fixed narrow spectral bandwidth. The limitation could be relieved if the electromagnetic response characteristics of the metamaterials can be dynamically tuned.

In the recent literature, a few papers have appeared on tunable metamaterials. Calculations and experiments performed at the microwave and infrared regimes have established that metamaterials can be adjusted by mounting variable capacitance diodes, photosensitive semiconductors, or ferroelectric capacitances to their inner structures [14-17]. The birefringence of liquid crystals (LCs) is well known and extensively used in optoelectronic systems for control and manipulation of visible, infrared, and millimeter wave beams. Indeed, LCs stand out as the preferred means of achieving tunability due to their feature of very large dielectric anisotropy sensitive to external fields. By changing the orientation of LCs incorporated with various resonators, the magnetic resonance can be controlled to achieve the reconfiguration of the negative index or permeability metamaterials [18-20]. In short, tunability is introduced by ensuring that the attached components are made of varactors, photocapacitances, ferroelectricities, LCs, etc.

In this study, four known design approaches of SRR structures [1-3,9] were analyzed and compared to further maximize the tuning effect of artificial magnetism. A new tunable negative permeability metamaterial, which

consists of a periodic array of SRRs and the multilayered substrates infiltrated with nematic LCs, will be presented. The dependence of the resonance frequency for various SRRs on some factors will be investigated, including the ring diameter, the radial and azimuthal gap, the electric permittivity and the thickness of the substrate, and the director orientation of the embedding LCs. The effective electromagnetic parameters are retrieved from the simulated transmission properties of an elementary SRR cell. The simulated resonance frequency and retrieval of the effective permeability characteristics will be discussed on the basis of the tuning in the director axis orientation angle of LCs. It can be seen that the magnetic resonance frequency is very sensitive to the variation of the electromagnetic properties of the substrate, especially for the geometry of the two-slit SRR (TSRR). By using an external field to control the LC molecular orientation, the TSRR structure yields a much better tunability on the frequency shift of the magnetic resonant response.

2. Design and study of SRR structures

The initial models of the composite negative magnetic permeability media are treated for the investigation of the magnetic resonance response. As shown in Fig. 1, there are four kinds of SRRs from which the various resonators are constructed. The basic unit cells are composed of a single-slit SRR (SSRR), a TSRR, a double-ring SRR (DSRR), and a modified SRR (MSRR), respectively. Using a shadow mask/etching technique, printed circuit boards with SRRs can be fabricated on one side or two sides. The original dimensions of the four SRR structures are indicated in the caption of Fig. 1 d is the width of the slit. All rings and substrates of the four SRRs have the same heights and thicknesses, respectively. The direction of electromagnetic wave propagation and the electric field are parallel to the SRR plane. The SRR resonance is excited by the magnetic field parallel to the ring axis.

For the analysis of the resonance characteristics in the SRR structures, electromagnetic simulations are performed by using the commercial software HFSS™, which is a three-dimensional full-wave solver employing the finite element method (FEM). In order to determine the resonance frequencies of the structures under consideration, the SRR cell shown in Fig. 2 is included along the propagation direction. The outer box with one layer of the SRR structures is the simulation zone, the size of which is 8×8×24 mm^3. The relative permittivity of the substrate is 3.8 and the relative permeability is 1. In addition, the dielectric loss tangent is fixed to be 0.02. The structures are subjected to an incident plane wave along the *y* axis from left to right. The *E* and *H* fields are polarized along the *x* and *z* axes, respectively. Absorption boundary conditions are employed along the propagation direction to limit the calculation space. Periodic boundary conditions are used along the directions other than the propagation direction.

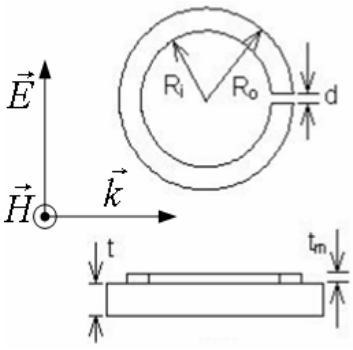

a

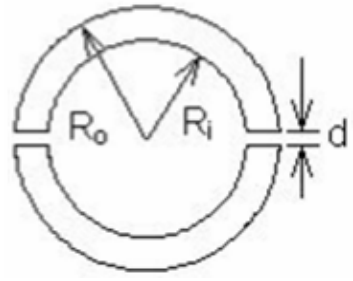

b

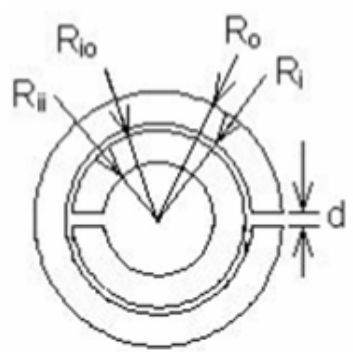

c

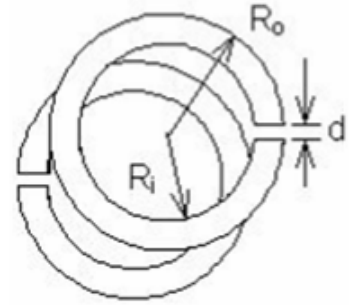

d

Fig. 1. Schematic representation of the SRR elements: (a) single-slit SRR (SSRR); (b) two-slit SRR (TSRR); (c) double-ring SRR (DSRR); (d) modified SRR (MSRR). The dimensions chosen for numerical calculations are R_i= 2.7 mm, R_o= 3.6 mm, R_{io}= 2.5mm, R_{ii}= 1.6mm, t= 0.25 mm, and t_m= 0.017 mm under the scale factor sc=1. The relative permittivity and the dielectric loss tangent of the substrate are 3.8 and 0.02, respectively.

The transmission spectrum can be extracted from the *S*-parameter calculation. For the microwave frequency, the rings are assumed to be made of perfect electrical conductors so that the salient features of transmittance might be visualized. The electromagnetic properties of the SRR system can be characterized in terms of an effective permeability μ_{eff} and permittivity ε_{eff} when the structure varies spatially on a scale much less than the incident radiation. In order to retrieve the effective permeability and permittivity, we need to characterize the SRR system as an effective homogeneous slab. The complex magnetic permeability and electric permittivity obtained via the *S*-parameter retrieval methods are given by [21]

$$\mu_{eff} = NZ \quad \text{and} \quad \varepsilon_{eff} = N / Z , \tag{1}$$

where

$$N = \cos^{-1}((1 - S_{11}^2 + S_{21}^2) / 2S_{21}) / kL , \tag{2}$$

and

$$Z = \sqrt{[(1+S_{11})^2 - S_{21}^2] / [(1-S_{11})^2 - S_{21}^2]} . \tag{3}$$

Here, S_{11} is equal to the reflection coefficient, S_{21} is related to the transmission coefficient, k is the incident wavenumber, and L is the thickness of the slab. N and Z are the effective refractive index and wave impedance of the slab, respectively.

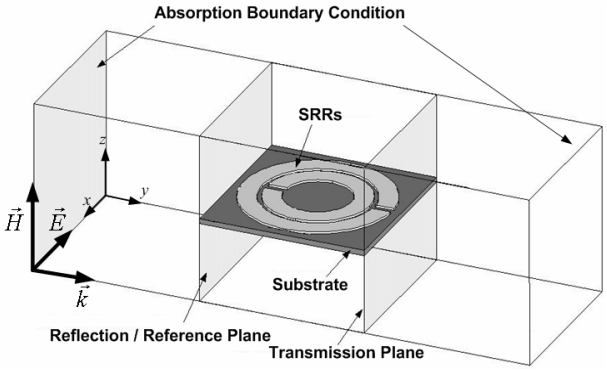

Fig. 2. Illustration of the SRR unit cell for simulations. The outer box size is 8 × 8 × 24 mm³. The periodic boundary conditions are in the x and z directions.

3. Comparison of resonant response

To maximize the accommodation of artificial magnetism, the magnetic particles in Fig. 1 were compared in the variation of the geometric dimensions. The numerical results for the resonance frequencies were obtained from the transmission spectra of the four SRR structures. The various sets of parameters applied to compare the tuning effect were investigated through electromagnetic simulations using the FEM tool. A scaled set of SRR dimensions is based on the scale factor *sc* given by

$$sc = D_{\text{curr}}/D_{\text{orig}} ,$$

where D_{orig} represents the parameters of the original structure for the dimensions of R_i, R_o, R_{io}, and R_{ii} depicted in the caption of Fig. 1. D_{curr} denotes the parameters of the scaled structure. As Fig. 3 demonstrates, the scaled down sets of dimensions for all types of SRRs cause the blue-shift effect of the magnetic resonance frequency. Under different slit widths (from the bottom limit d_B to the top limit d_T), simulation results show that increasing the slit widths increases the resonance frequency of the SRR structure. For $d=0.1528R_o$ in all the cases, the log-log plot of the resonance frequency versus the scale factor *sc* shows approximately linear curves with the same slope of about -0.98, which is characteristic of the particular scaling design. As SRRs can be modeled as *LC* circuits, circuit theory then predicts a resonance frequency $\omega_m = (L_{eff} C_{eff})^{-1/2}$ determined by the effective inductance L_{eff} from the metal rings and the effective capacitance C_{eff} through the slits in the rings or the gaps between the rings. The capacitance scales proportionally to SRR size, provided that all SRR dimensions are scaled down simultaneously. However, the slit capacitance scales inversely with the width of the slit, and the effective capacitance can be reduced by introducing further slits into the ring [22]. As shown in Fig. 3 for the two cases of SSRRs and TSRRs, the resonance frequency increases with the number of cuts in the SRR. In particular, the magnetic response of the SRRs is dominated by the slit capacitance [14]. TSRRs possess a larger adjusting range in connection with the variance of the slit capacitance. It should be clear that the magnetic resonance frequency could be further increased by reducing the net capacitance, especially for the case of TSRRs.

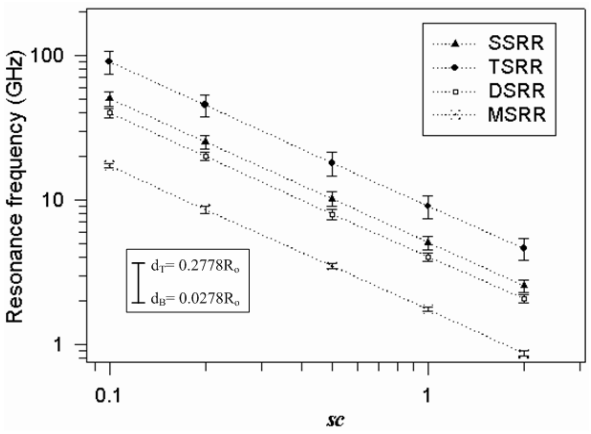

Fig. 3. Dependence of the magnetic resonance frequency on the scalar factor sc for the four kinds of SRRs. Error bars indicate the variation of the width d of the slit between the top limit d_T and the bottom limit d_B.

The effects of the substrate dielectric permittivity and physical thickness on the effective properties of the SRR metamaterials were studied from the computed *S*-parameters. Fig. 4 shows the dependence of the resonance frequency on the substrate permittivity through examining the transmission minimum. The thickness and the dielectric loss tangent of the substrate are fixed at t= 0.25 mm and 0.02, respectively. It can be seen that the resonance frequencies vary apparently with the dielectric property of the substrate, especially for the model of TSRRs, in which the frequency descends from ~11.65 to ~3.49 GHz (the real part of the electric permittivity increases from 1 to 30). The resonance frequency can be lowered by increasing the dielectric constant of the substrate, and thus, can be controlled by varying the dielectric properties of the substrate. Further, the thickness of the substrate is also altered to examine the effect on the magnetic resonance frequency. The response of the resonance frequency varying with the substrate thickness is shown in the inset of Fig. 4. The relative permittivity of the substrate is selected to be 3.8. Except the case of MSRRs, the resonance frequency drops as the substrate thickness increases. For the MSRR structure, raising the substrate thickness decreases the effective capacitance between the rings so that the resonance frequency increases with the thickness. It is also noticed that the resonance frequencies become saturated as the substrate thickness is beyond 1.1 mm for all the cases. Irrespective of the increment of the substrate thickness, the field caused by the distributed capacitors is localized in a small region, so the change of the effective capacitance becomes less and trends to saturate.

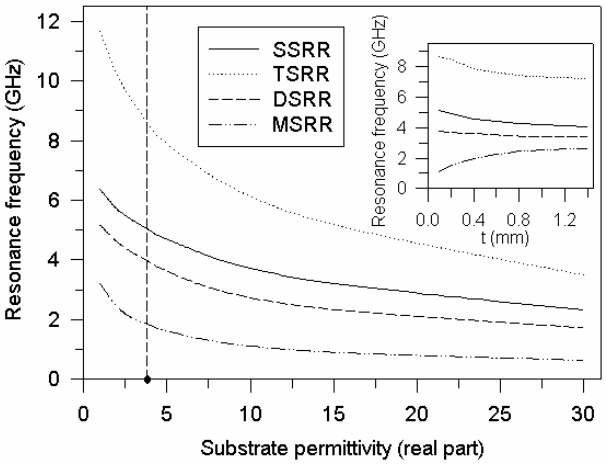

Fig. 4. Variation of the magnetic resonance frequency with the real part of the substrate permittivity for the four kinds of SRRs (d= 0.2 mm). The inset shows the dependence of the magnetic resonance frequency on the substrate thickness with the substrate permittivity indicated by the vertical dash-line.

4. Tunable negative permeability metamaterials based on LCs

On the whole, the most important factor for the metamaterial design to characterize the SRRs is approximately the magnetic resonance frequency. The model of TSRRs analyzed in Figs. 3 and 4 seems to be the favorable candidate for being a SRR with a broad tuning range of negative permeability at resonance. Fig. 5 shows the illustration of the basic unit of the tunable metamaterial, which consists of TSRR patterns printed on the surface of the sandwich glass slabs with infiltration of LC mixtures in between. Such a design compared with other configurations [19,20] can reduce the usage of LCs and relax the cost. The LC director lies in the *x*-*z* plane. The director axis **n** can take all values $\{\sin\theta, 0, \cos\theta\}$ by applying a magnetic or an electric field based on the Fréedericksz effect, where θ denotes the rotation angle of the molecular director with respect to the *z* axis. The width of the slits is d= 0.4 mm. The other geometric parameters are the same as the dimensions listed in the caption of Fig. 1. To widen the tuning range, advanced nematic LC mixtures doped with tiny ferroelectric particles have been proposed, and their electromagnetic properties can reveal much higher dielectric anisotropy [23]. In the following analysis on this basis, $\varepsilon_e = 17$ and $\varepsilon_o = 4$ were taken to describe the LC medium, where ε_e and ε_o are the relative permittivities parallel and perpendicular to the molecule director, respectively. It is assumed that the voids infiltrated with LCs are untreated on the surface. When no external field is applied, the LC can be treated as a homogeneous isotropic material with an average dielectric constant of $\varepsilon = (2\varepsilon_o + \varepsilon_e)/3$. Through the identical computation model shown in Fig. 2, a full wave analysis using the FEM was performed to determine the transmission property and the tunability of highly anisotropic metamaterials embedding LCs.

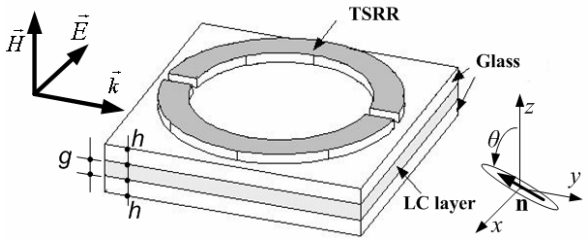

Fig. 5. Illustration of the TSRR unit cell of the tunable negative permeability metamaterial infiltrated with LCs. The LC molecule director lies in the x-z plane.

The effect of the LC layer thickness on the resonance frequency as well as the LC orientation was studied numerically by considering two different thicknesses of the glass slabs. In Fig. 6, the resonance frequencies are provided for the four cases, the two glass thicknesses of

h=0.1 and 0.2 mm in regard to the LC director along the z axis (θ=0°, $\varepsilon_z = \varepsilon_e$, $\varepsilon_x = \varepsilon_y = \varepsilon_o$) and the x axis (θ=90°, $\varepsilon_x = \varepsilon_e$, $\varepsilon_y = \varepsilon_z = \varepsilon_o$), with the change of the LC layer thickness g varying from 0.1 to 1.5 mm. Application of an external field will orient the LC molecules along the field direction. It should be mentioned that not only the slit capacitance has the contribution to the total capacitance of the SRR system, but also the variation of the fringe capacitance near the slit will greatly affect the effective capacitance of the system [19]. Under specified thicknesses of the LC layer and the glass slab, as the LC director is reorientated from θ=0° to θ=90°, the change of ε_x from ε_o to ε_e increases the fringe capacitance as shown in the inset of Fig. 6. Thus, the increase of the capacitance results in the red-shift of the resonance of TSRRs. It is also noticed that the resonance frequencies with respect to the increase of the LC layer thickness become saturated and are similar to the results of the inset in Fig. 4. The saturation reveals that the effect of the fringe capacitance is limited to a small range near the slit. Besides, increasing the director angle from θ=0° to θ=90° for the 0.2 mm glass slabs could gain a maximum shift of the resonance frequency from 8.62 to 7.83 GHz when the LC layer thickness is fixed at g=0.4 mm. Further, the LC layer thickness of g=0.3 mm under h=0.1 mm could provide a much larger range of 8.92-7.82 GHz for the tuning purpose. The decrease of the glass slab thickness could expand the tunability of the magnetic metamaterial.

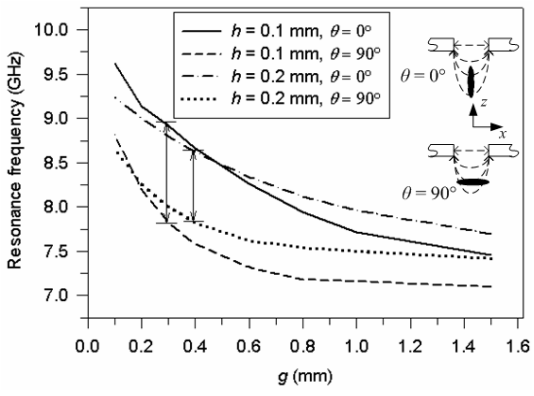

Fig. 6. Dependence of the magnetic resonance frequency on the thickness of the nematic LC layer with respect to the different molecule orientations at θ= 0° and 90° under the two glass slab thicknesses of h = 0.1 and 0.2 mm.

According to the optimal conditions of the maximum tuning range, Fig. 7 shows the simulated *S*-parameters and the retrieved effective permeability of the tunable TSRR model for different LC orientations under the two different glass permittivities of ε_g= 3.8 and 2.5. The resonance dips in the transmission spectra are caused by the intrinsic resonance of SRRs. For the LC influence on magnetic resonance, the tunable metamaterial exhibits negative permeability values in the frequency band ranging from ~8.94 to ~9.12 GHz (~9.82 to 10.02 GHz) for the case of θ=0° in Fig. 7(a) (Fig. 7(b)). By increasing the director angle to θ=90°, a clear red-shift of the frequency band with negative permeability down to 7.85-7.98 GHz (8.69-8.86 GHz) can be observed in Fig. 7(a) (Fig. 7(b)). In brief, the total fringe capacitance can be divided into the capacitances of the glass slab and the LC layer, which are connected in parallel to the slit capacitance, respectively. The decrease in the dielectric constant of the glass slab that yields the reduction of the total fringe capacitance will reduce the effective capacitance of the SRR system to result in the blue-shift effect of the resonance frequency as shown in Figs. 7(a) and (b).

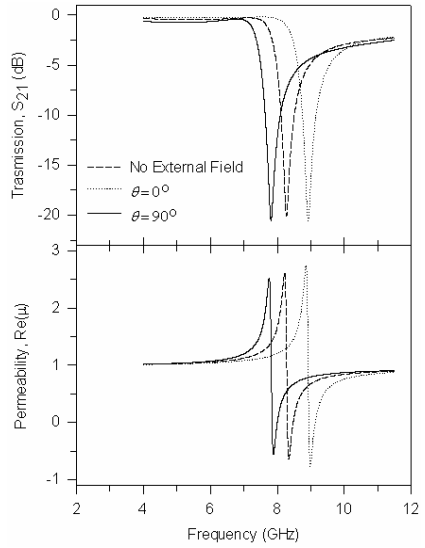

a

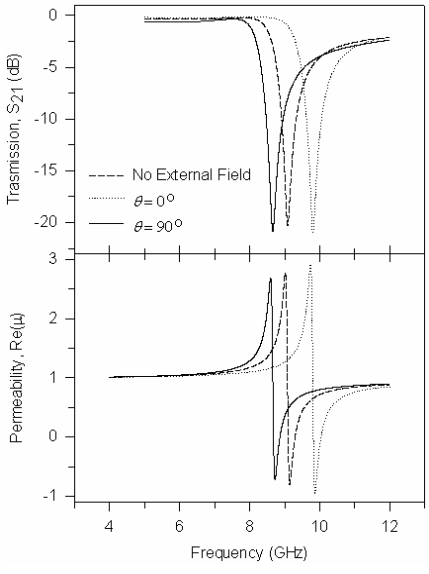

b

Fig. 7. Transmission spectra for arrays of TSRRs and the corresponding effective permeability obtained by the retrieval methods under different LC orientations. (a) ε_g= 3.8 and (b) ε_g= 2.5 are the two different dielectric constants of the glass slabs. (h= 0.1 mm, g=0.3 mm).

At different dielectric constants of the glass slabs, the magnetic resonance frequencies and their corresponding effective permeabilities of the TSRR system as a function of the LC director angle are shown in Fig. 8. In both the cases, the magnetic resonance frequency is gradually decreased with the LC director angle. In contrast, the real part of the effective permeability at its corresponding resonance frequency shifts toward higher values as the LC director angle is increased from 0° to 90°. The tuning range depends on the manipulation of the substrate permittivity, the dielectric permittivity difference in nematic LC compounds, and the thicknesses of the LC layer and the glass slab.

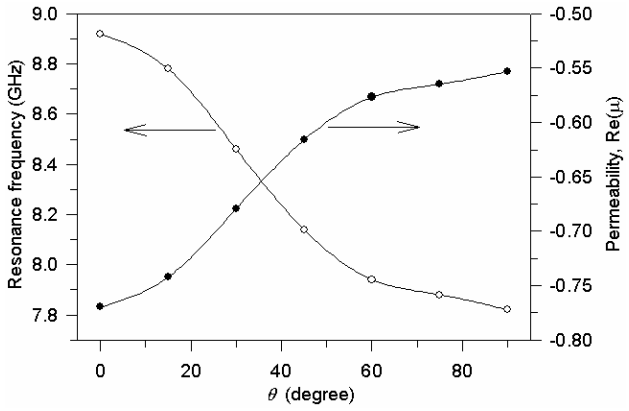

a

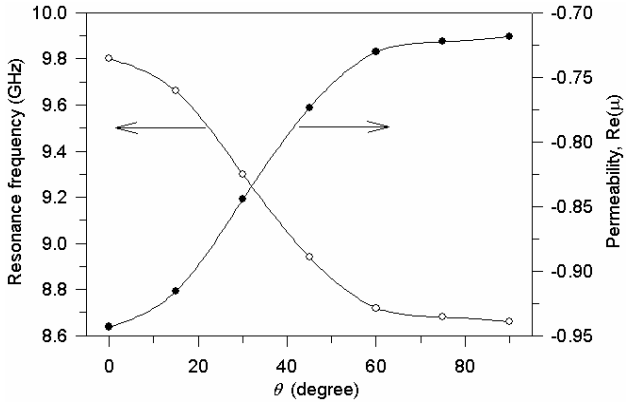

b

Fig. 8. The magnetic resonance frequency and the corresponding effective permeability as a function of the reorientation angle of the LC molecules. (a) and (b) are the same cases as Figs. 7(a) and (b).

5. Conclusions

In summary, a comparative analysis of the magnetic resonance characteristics of SRRs with various configurations has been carried out in this study. It has been found that TSRRs could provide a larger shift in the magnetic resonance frequency with respect to the SRR size scaling, the split width and the substrate permittivity. Thus, such a TSRR configuration could have the advantage for the tuning purpose. Based on the TSRR structure incorporating anisotropic LCs, a reconfigurable metamaterial design has been also presented for adjusting the resonance conditions and the negative permeability. By using the simulated scattering parameters, it has been shown that the broad tunability of the magnetic resonance frequency can be conveniently realized by changing the director orientation of the LC molecules via altering the applied external fields. The TSRR structure infiltrated with LCs could provide an effectual way of controlling the location of the negative-index-metamaterial band and would be useful for the construction of novel devices.

Acknowledgements

The authors would like to thank the National Science Council (NSC) and the Ministry of Economic Affairs of Taiwan for financial support under Grant Nos. NSC 97-2221-E-432-001 and 97-EC-17-A-07-S1-0018.

References

[1] J. B. Pendry, Contem. Phys. **45**, 191 (2004).
[2] J. García-García, J. Bonache, I. Gil, F. Martín, R. Marqués, F. Falcone, T. Lopetegi, M. A. G. Laso, M. Sorolla, Microwave Opt. Tech.Lett. **44**, 376 (2005).
[3] S. Maslovski, P. Ikonen, I. Kolmakov, S. Tretyakov, M. Kaunisto, Prog. In Electromagn. Res. **54**, 61 (2005).
[4] H. Chen, L. Ran, J. Huangfu, X. Zhang, K. Chen, T. M. Grzegorczyk, J. A. Kong, Appl. Phys. Lett. **86**, 151909 (2005).
[5] A. K. Azad, J. Dai, W. Zhang, Opt. Lett. **31**, 634 (2006).
[6] K. Aydin, Z. Li, M. Hudlička, S. A. Tretyakov, E. Ozbay, New J. Phys. **9**, 326 (2007).
[7] R. S. Penciu, K. Aydin, M. Kafesaki, Th. Koschny, E. Ozbay, E. N. Economou, C. M. Soukoulis, Opt. Express **16**, 18131 (2008).
[8] J. Zhang, H. Chen, L. Ran, Y. Luo, B.-I. Wu, J. A. Kong, Appl. Phys. Lett. **92**, 084108 (2008).
[9] E. Plum, V. A. Fedotov, N. I. Zheludev, Appl. Phys. Lett. **93**, 191911 (2008).
[10] C. Caloz, T. Itoh, Electromagnetic Metamaterials: Transmission Line Theory and Microwave Applications, Wiley, Hoboken (2006).
[11] K. B. Alici, E. Ozbay, J. Appl. Phys. **101**, 083104 (2007).
[12] Z. Liu, H. Lee, Y. Xiong, C. Sun, X. Zhang, Science **315**, 1686 (2007).
[13] W. Cai, U. K. Chettiar, A. V. Kildishev, V. M. Shalaev, Nature Photon. **1**, 224 (2007).

[14] K. Aydin, E. Ozbay, J. Appl. Phys. **101**, 024911 (2007).
[15] A. Degiron, J. J. Mock, D. R. Smith, Opt. Express **15**, 1115 (2007).
[16] A. Marteau, G. Velu, G. Houzet, L. Burgnies, E. Lheurette, J. C. Carru, D. Lippens, Appl. Phys. Lett. **94**, 023507 (2009).
[17] N.-H. Shen, M. Kafesaki, T. Koschny, L. Zhang, E. N. Economou, C. M. Soukoulis, Phys. Rev. B **79**, 161102 (2009).
[18] X. Wang, D.-H. Kwon, D. H. Werner, I.-C. Khoo, A. V. Kildishev, V. M. Shalaev, Appl. Phys. Lett. **91**, 143122 (2007).
[19] F. Zhang, Q. Zhao, D. P. Gaillot, X. Zhao, D. Lippens, J. Opt. Soc. Am. B **25**, 1920 (2008).
[20] F. Zhang, L. Kang, Q. Zhao, J. Zhou, X. Zhao, D. Lippens, Opt. Express **17**, 4360 (2009).
[21] D. R. Smith, D. C. Vier, Th. Koschny, C. M. Soukoulis, Phys. Rev. E **71**, 036617 (2005).
[22] J. Zhou, Th. Koschny, M. Kafesaki, E. N. Economou, J. B. Pendry, C. M. Soukoulis, Phys. Rev. Lett. **95**, 223902 (2005).
[23] O. Buchnev, E. Ouskova, Yu. Reznikov, V. Reshetnyak, H. Kresse, A. Grabar, Mol. Cryst. Liq. Cryst. **422**, 47 (2004).

*Corresponding author: n1888112@nckualumni.org.tw
mecjy@mail.hku.edu.tw